JOURNAL OF GEOPHYSICAL RESEARCH, VOL. 93, NO. D6, PAGES 7015–7025, JUNE 20, 1988

# Evidence of Gravity Wave Saturation and Local Turbulence Production in the Summer Mesosphere and Lower Thermosphere During the STATE Experiment

DAVID C. FRITTS AND STEVEN A. SMITH[1]

*Geophysical Institute and Department of Physics, University of Alaska, Fairbanks*

BEN B. BALSLEY

*Aeronomy Laboratory, National Oceanic and Atmospheric Administration, Boulder, Colorado*

C. RUSSELL PHILBRICK

*Air Force Geophysics Laboratory, Hanscom Air Force Base, Bedford, Massachusetts*

This study utilizes the unique data set obtained during the Structure and Atmospheric Turbulence Environment (STATE) experiment, conducted during June 1983 at Poker Flat, Alaska, to examine the structure and characteristics of the wave field near the summer mesopause. It is shown that the rocket and radar data together permit a much more detailed specification of wave parameters than would be possible using either data set alone. The results of this analysis suggest that the wave field near the summer mesopause is composed, in general, of a superposition of wave motions which act collectively to produce regions in which the wave field is convectively or dynamically unstable. These regions are found to correlate well with zones of enhanced turbulence and small-scale wave activity, suggesting the processes and effects of wave field saturation.

## 1. INTRODUCTION

There has been a resurgence of interest in the last few years in the propagation and saturation of gravity waves in the middle atmosphere, following the recognition of their role in establishing the large-scale circulation and thermal structure of this region [*Houghton*, 1978; *Lindzen*, 1981]. Initial modeling studies by *Matsuno* [1982], *Holton* [1982, 1983], and *Dunkerton* [1982*a*] showed that crude parameterizations of gravity wave drag and induced diffusion could account for several significant features of the middle atmosphere circulation and structure. These include the reversals of the vertical shear of the mean zonal wind and of the mean meridional temperature gradient in the mesosphere. Similar results were obtained in a high-resolution study by *Miyahara et al.* [1986] that employed direct simulation of gravity wave motions. Other theoretical studies addressed several aspects of gravity wave propagation and saturation of relevance to this observational study, including effects of wave-wave and wave-mean flow interactions [*Weinstock*, 1982; *Dunkerton*, 1982*b*; *Walterscheid*, 1984; *Fritts*, 1985], convective adjustment of unstable wave fields [*Dunkerton and Fritts*, 1984], and the induced diffusion of heat and constituents [*Schoeberl et al.*, 1983; *Chao and Schoeberl*, 1984; *Fritts and Dunkerton*, 1985; *Strobel et al.*, 1985].

In contrast to the relatively large number of theoretical studies of gravity wave propagation and saturation, only a few observational studies have been performed that specifically address gravity wave saturation and its effects. A measure of the zonal drag due to saturating gravity waves as well as phase speed, period, and wavelength estimates were provided by *Vincent and Reid* [1983]. Related studies by *Smith and Fritts* [1983], *Balsley et al.* [1983], *Meek et al.* [1985*a*], *Smith et al.* [1987], *Fritts and Vincent* [1987], and *Reid and Vincent* [1987*a*, *b*] provided information on gravity wave scales, amplitudes, and fluxes, as well as the conditions leading to saturation of the gravity wave spectrum. Additional evidence of saturation and of characteristic wave amplitudes and their variability were presented by *Vincent* [1984], *Meek et al.* [1985*b*], and *Vincent and Fritts* [1987]. The initial theoretical and observational studies of gravity waves in the middle atmosphere were reviewed by *Fritts* [1984*a*].

Most previous studies of gravity waves in the middle atmosphere have used data from a single observing system. This usually provides information on only a single variable (velocity, temperature, or density) and causes some ambiguity in the description of the gravity wave field. When two or more instrument systems are used together, however, a much more complete determination of the wave field and its middle atmosphere effects can be obtained. Such was the case in the Structure and Atmospheric Turbulence Environment (STATE) experiment, which provides the basis for this series of papers.

The simultaneous and nearly colocated radar and rocket data collected during the STATE experiment provide a unique opportunity for a detailed look at the role played by gravity waves in middle atmosphere dynamics. As will be seen later, this data facilitates the inference of gravity wave scales, directions of propagation, mechanisms, and likely consequences of dissipation as well as the middle atmosphere response. Of particular interest in the STATE experiment are an explanation for the very strong MST radar echoes observed near

[1]Now at NASA Marshall Space Flight Center, Huntsville, Alabama.



Paper number 7D0518.
0148-0227/88/007D-0518$05.00

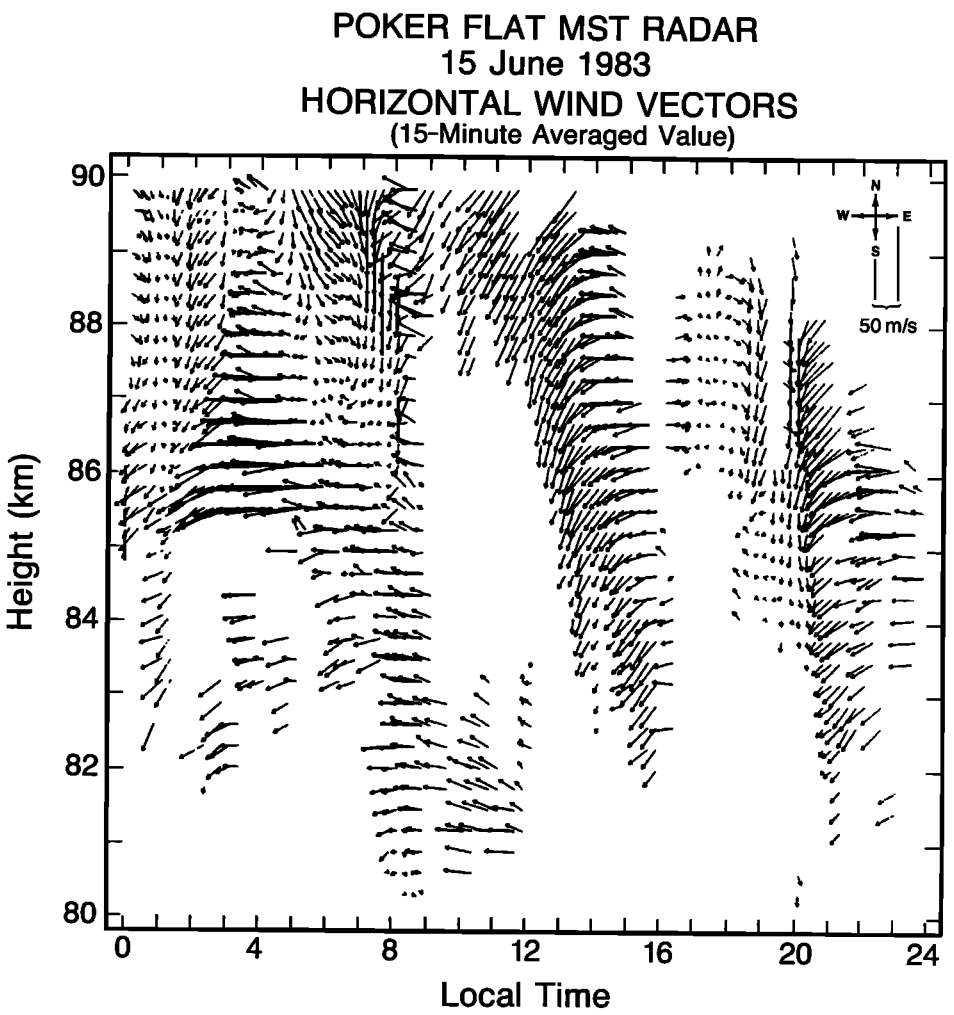


Fig. 1. Time-height cross section of the inferred horizontal wind field for June 15, 1983. Each vector represents a 15-min average. Note the low-frequency motion dominating the last half of this interval.

the summer mesopause and the mechanism or mechanisms that provide a large energy dissipation rate ($\varepsilon$) and a small Kolmogorov inner scale ($l_0$) in that region. Estimates of these quantities during the STATE experiment are provided by *Watkins et al.* [this issue], *Kelley et al.* [this issue], and *Ulwick et al.* [this issue]. In addition, this data will help us to assess the validity of the various theories that have been advanced to account for previous gravity wave observations and their middle atmosphere effects.

An overview of the STATE data used in the wave field analysis is presented in section 2. A significant feature of these data is the very high degree of spatial and temporal variability. An elementary discussion of gravity wave structure and of the relationship between the various wave parameters observed with the radar and rocket instrumentation is provided in section 3. This suggests some redundancy in our ability to estimate various gravity wave parameters. The analysis of the wave field observed during salvo 2 is presented in section 4. These data provide clear evidence of both large- and small-scale wave motions throughout the height interval over which data were collected. The large-scale motion is observed in both velocity and temperature fields and is seen to correlate well with the radar signal-to-noise (S/N) data and regions of enhanced small-scale wave amplitudes, suggesting that instability and dissipation are highly localized within the wave field. A second event yielding a similar correlation is described in section 5. The conclusions of this study are presented in section 6.

## 2. Data Overview

The objectives of the STATE experiment and discussions of the rocket and radar data collected are presented in other papers in this series. The purpose of this section is to review that portion of the data that can be used to infer the characteristics and effects of observed internal gravity wave motions.

Perhaps the most striking feature of the radar data collected near the summer mesopause at Poker Flat is the enormous temporal variability of the velocity field. The time-height cross sections of the 15-min average inferred horizontal wind between 80 and 90 km are shown for June 15 and 17, 1983, in Figures 1 and 2. The first of these exhibits relatively high-frequency motions ($T \lesssim 2$ hours) at upper levels from 0000 to 0800 LT. Thereafter the motion field is dominated by a low-frequency wave ($T \sim 7$ hours), which rotates anticyclonically with time and height, suggestive of the low-frequency tidal and gravity wave motions considered by *Balsley et al.* [1983]. The occurrence of strong radar echoes is seen to be highly corre-

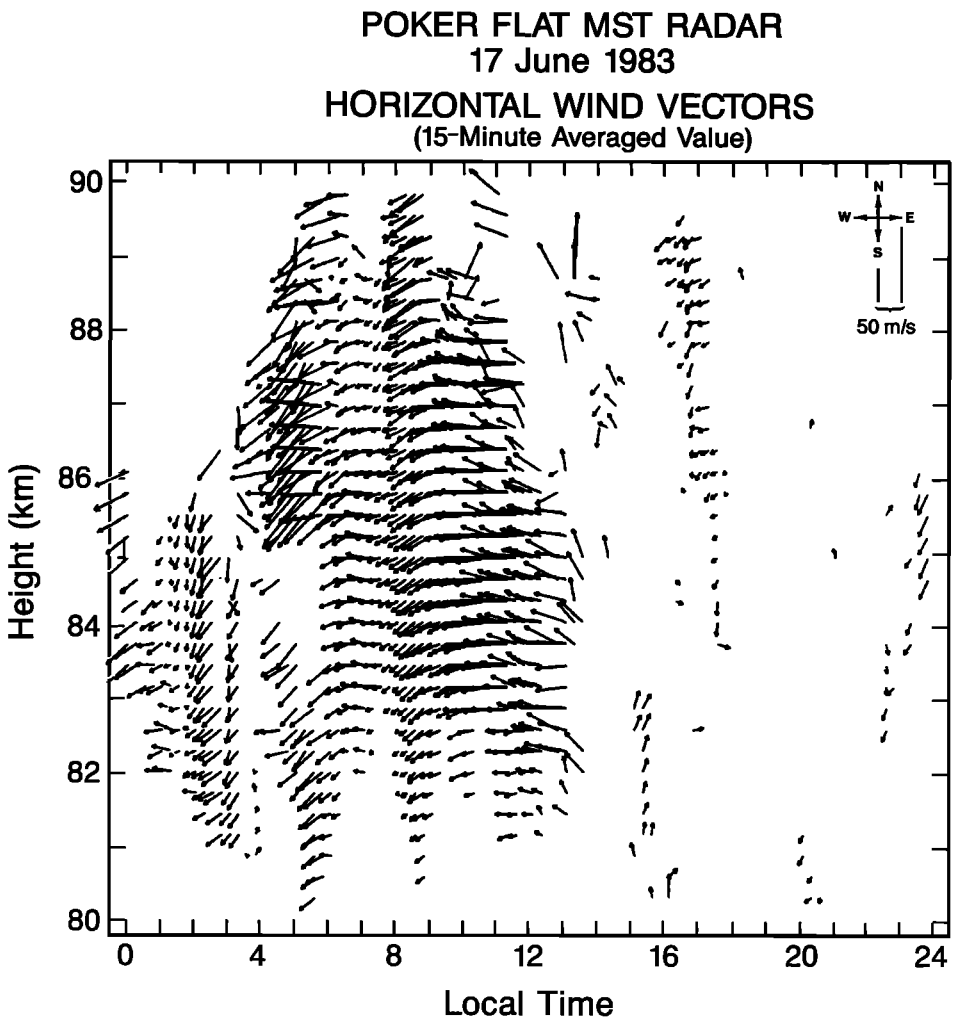


Fig. 2. As in Figure 1, for June 17. Note here the ~3-hour modulation of the velocity field and of the lowest echoing levels.

lated with a particular phase of this wave motion. The motion field on June 17 (see Figure 2) exhibits a dominant wave with $T \sim 3$ hours up to ~1200 AST. After that time, echoes are sufficiently sparse that no wave motion can be discerned. As in the case of the ~7-hour wave, the phase of the ~3-hour wave motion appears to be correlated with the occurrence of strong echoes at lower levels. Unlike the previous example, no low-frequency motions are apparent on this day.

A complementary data set is provided by the rocket wind and temperature observations obtained with the Nike-Hydac instrument package launched at 2051 LT during salvo 2 on June 15. This data set, while not providing any information on the temporal evolution of the wind and temperature fields, does provide comprehensive data on the vertical structure and the amplitudes of various scales of motion at a particular time over a height range of 55–130 km. The zonal and meridional wind profiles and the temperature profile obtained with the Nike-Hydac are shown in Figures 3 and 4.

The dominant vertical scales in the two velocity profiles are in the range ~5–15 km, with smaller-amplitude motions (with $\lambda_z \lesssim 2$ km) at lower levels and large-scale ($\lambda_z \sim 30$ km) and large-amplitude motion apparent at upper levels. Overall, it is the larger amplitudes associated with the larger vertical scales that appear to be most significant here.

The temperature data shown in Figure 4, in contrast to the velocity data, suggest that motions with both large and small vertical scales contribute appreciably to temperature fluctuations, with the maximum gradients associated primarily with the minimum vertical scales. As will be seen in section 3, it is the temperature gradient that determines whether a particular wave motion is stable or (convectively) unstable.

Thus the velocity and temperature data provide us with two different views of the same wave field. It will be shown in section 3, however, that these two fields permit a much more complete specification of wave parameters and propagation characteristics than is possible with either field alone. In some instances, in fact, the two sets of data are redundant and constitute a test of the experimental techniques.

## 3. Gravity Wave Structure

The purposes of this section are to review linear gravity wave structure and to demonstrate what wave parameters can be inferred using the radar and rocket velocity and temperature data collected during the STATE experiment. The results will then be employed in section 4 to examine the structure and evolution of the gravity wave field.

Throughout much of the middle atmosphere, the mean state

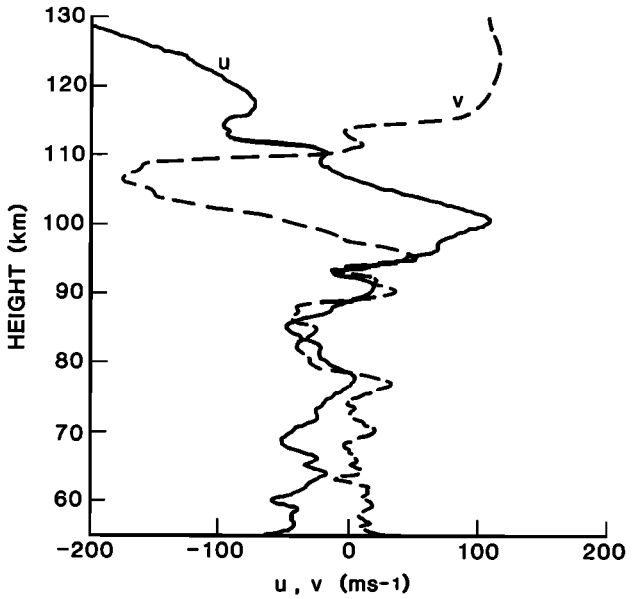


Fig. 3. Zonal and meridional velocity profiles derived from the three-axis accelerometer data obtained during Salvo 2 on June 15.

is characterized by a large Richardson number,

$$Ri_0 \equiv \frac{N^2}{(\bar{u}_z^2 + \bar{v}_z^2)} \gg 1 \tag{1}$$

where $N$, $\bar{u}_z$, and $\bar{v}_z$ are the Brunt-Väisälä frequency and the mean zonal and meridional wind shears, respectively. Under these conditions, gravity wave parameters vary little over a vertical wavelength and are described well by WKB theory. In addition, we assume intrinsic frequencies (i.e., those measured relative to the local mean flow) such that

$$f^2 \ll \omega^2 \equiv k^2(c - \bar{u})^2 \ll N^2 \tag{2}$$

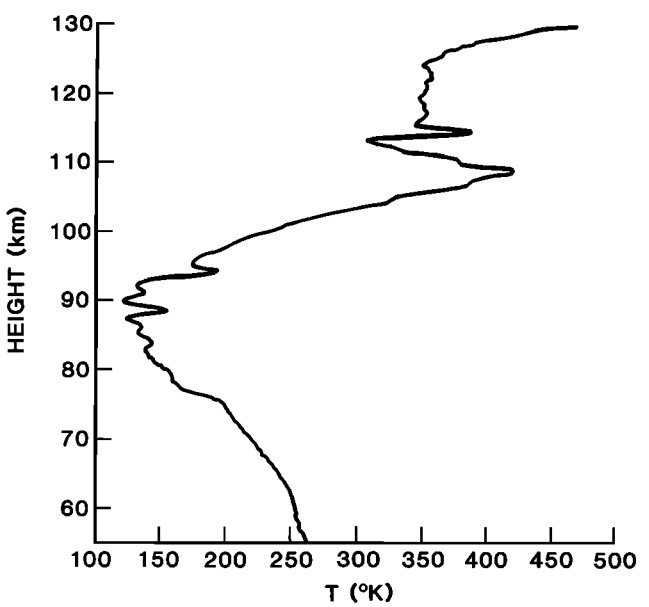


Fig. 4. Temperature profile derived from the three-axis accelerometer data obtained during Salvo 2 on June 15. Note the conspicuous ~30-km wavelength at upper heights.

and vertical wavelengths which satisfy

$$\lambda_z^2 \ll (4\pi H)^2 \tag{3}$$

where $f$ is the inertial frequency, $k(=2\pi/\lambda_x)$ is horizontal wave number, $c$ is phase speed, $\bar{u}$ is the mean flow in the direction of wave propagation, and $H$ is the atmospheric scale height. Then the vertical wave number is simply

$$m = 2\pi/\lambda_z = \pm N/(c - \bar{u}) \tag{4}$$

Thus provided the mean atmospheric stratification is known, measurement of the vertical wavelength of a gravity wave implies knowledge of the intrinsic phase speed, $c - \bar{u}$, of the motion.

Now assuming a wave motion of the form

$$\phi' = \phi_0 \exp [i(kx + mz - kct)] \tag{5}$$

the linear thermodynamic energy and continuity equations yield

$$\theta_z'/\bar{\theta}_z = u'/(\bar{u} - c) \tag{6}$$

Thus a wave motion achieves a state of convective instability (where $\theta_z' \leqq -\bar{\theta}_z$) at the level of maximum horizontal velocity in the direction of wave propagation. For motions with $\omega \gg f$, this corresponds to the condition

$$u_z' > N \tag{7}$$

It must be noted, however, that the region of instability is expected where $\theta_z'$ is a minimum and $u'$ is a maximum, rather than in regions of maximum shear.

For gravity waves with intrinsic frequencies near $f$, the Coriolis acceleration becomes important, and the expression for vertical wave number becomes

$$m^2 = \frac{k^2(N^2 - \omega^2)}{(\omega^2 - f^2)} \approx \frac{k^2N^2}{(\omega^2 - f^2)} \tag{8}$$

Another consequence of rotation is a horizontal perturbation velocity transverse to the direction of wave propagation given by

$$v' = \frac{if}{\omega} u' \tag{9}$$

which approaches $u'$ in magnitude as $\omega \to f$. This altered wave structure results in enhanced velocity shears and suppressed thermal fluctuations for $\omega \sim f$, implying that such motions may become dynamically unstable at amplitudes smaller than those required for convective instability [see *Fritts and Rastogi*, 1985].

Regions of wave field instability in the middle atmosphere occur in response to several factors, including amplitude growth due to the decrease in atmospheric density with height, a reduction in the intrinsic phase speed due to propagation in a sheared environment, and a reduction of vertical wavelength due to an increase in atmospheric stability [*Balsley et al.*, 1983] or as a result of wave superposition. The resulting instabilities produce turbulence, which acts to restrain wave amplitudes. This contributes to the diffusion of heat and constituents and causes an acceleration of the local mean flow due to a divergence of the momentum flux of the gravity wave motions.

The gravity wave structure outlined above indicates that a number of important wave parameters can be inferred from the rocket and radar data collected during the STATE experi-

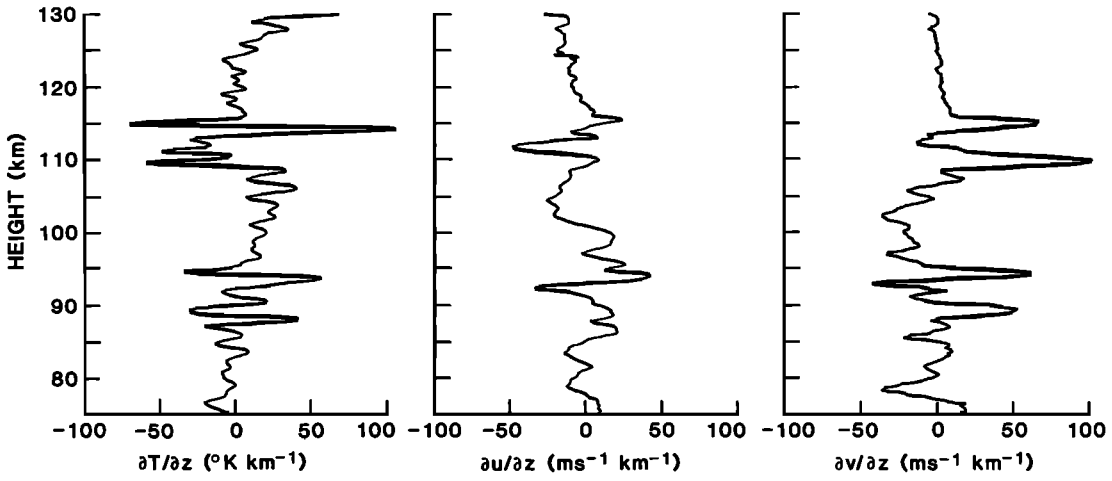


Fig. 5. Differenced temperature and velocity profiles. Note that the largest gradients are associated with small vertical wavelengths.

ment. The vertical wavelength can be measured using either rocket or radar data and also provides an estimate of the intrinsic phase speed, $c - \bar{u}$, using (4). Radar and rocket velocity data can be used to infer horizontal perturbation velocities, directions of propagation, and, together with the intrinsic phase speed, wave amplitudes relative to saturation values. The radar data also yield estimates of $kc$ and $\bar{u}$, and thus of $\omega$ and $\lambda_x$, using (4) and (9). Finally, the rocket temperature data facilitates estimates of $\theta'$ and $\theta_z'$, permitting a check on the wave amplitudes inferred from the velocity data. Thus subject to reasonable assumptions, all of the important parameters can be inferred for gravity waves that are sufficiently well defined in the STATE data. Several analyses which examine the evolution of the gravity wave field and its role in the generation of turbulence are presented in the following sections.

## 4. Analysis of Salvo 2 Wave Field Data

The most comprehensive data on the thermal and velocity fluctuations due to atmospheric wave motions obtained in the STATE experiment were those collected during salvo 2 on June 15. These data include radar-inferred horizontal and vertical velocities between ~80 and 90 km, with temporal and vertical resolutions of ~2 min and 300 m (see Figure 1), as well as rocket-inferred velocity and temperature data between 55 and 130 km with a height resolution of ~250 m (see Figures 3 and 4). As noted in section 2, these data display a range of wave motions occurring on various temporal and spatial scales. The analysis presented in this section will focus on those motions with vertical wavelengths of ~2, 12, and 30 km.

### 4.1. *The $\lambda_z \sim$ 30-km Wave*

We assume here that the fluctuations noted in the rocket and radar data presented in Figures 1–4 are a manifestation of internal gravity waves, in order to apply the results of section 3. This is almost certainly true for the small- and medium-scale motions ($\lambda_z < 20$ km). But for larger-scale motions ($\lambda_z \sim$ 30 km), there is a possibility that the fluctuations are due in part to tidal motions, with semidiurnal and terdiurnal components contributing preferentially. Because of the enormous daily variability of the low-frequency wave structure in the radar velocity field (there is no evidence of a low-frequency motion on June 17 in Figure 2) and the general consistency of the radar- and rocket-inferred wave parameters for the large-scale motion obtained in this section, however, we assume that gravity waves are the major contributor to the motion field near and above the mesopause. We recognize, nevertheless, that inferred wave parameters are likely influenced by tidal motions at upper levels to some degree.

By far the dominant wave structure apparent in the rocket velocity and temperature profiles is that with $\lambda_z \sim 30$ km, seen at upper levels in Figures 3 and 4. In order to obtain a reasonable fit to these data, we first difference each data set at a 250-m interval to remove the mean and linear trend. It is particularly important to remove the trend from the temperature data because of the rapid increase of temperature with height above the cold summer mesopause. The differenced profiles are displayed in Figure 5. As noted in section 2, the maximum temperature gradients are clearly associated with the smallest vertical wavelengths.

We assume a saturated (constant amplitude) wave motion with uniform structure above 85 km. This is appropriate because $N$ and $(c - \bar{u})$ do not change significantly in a vertical wavelength ($Ri_0 \gg 1$). We then fit the differenced velocity and temperature data only above the mesopause to insure that the temperature minimum at that height does not bias the amplitude or phase of the inferred temperature wave. The least squares fit to the differenced temperature data occurs for $\lambda_z =$ 30 km and is shown in Figure 6. The temperature amplitude of this wave is 59.7°C, with a maximum occurring at 107.9 km.

Similar fits to the differenced zonal and meridional velocity profiles were performed and the results tabulated in Table 1. The most notable feature of the velocity field, also apparent in Figure 3, is that the zonal and meridional velocities are nearly in quadrature and of comparable amplitude, suggesting a low-frequency motion with downward phase progression (and upward energy propagation). It must be cautioned, however, that there are potential errors in the amplitude and phase of the two velocity components, particularly the zonal, because of possible variations of the mean flow on the scale of the wave motion.

With both temperature and velocity perturbations specified, we are in a position to estimate the direction of propagation of the wave motion as well. This can be done either by determining the direction of the major axis of the velocity ellipse or

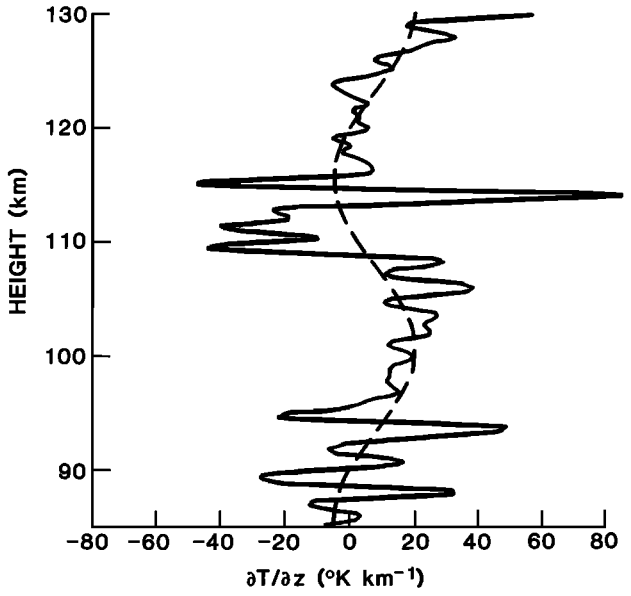


Fig. 6. Differenced temperature data and best fit to large-scale (30 km) wave motion. The amplitude of this motion is less than that required for convective instability.

from the relative phase of the temperature and velocity fluctuations. From the heights of maximum amplitude for the two velocity components, we infer a phase difference of 82°. This implies a maximum velocity of 82.5 m $s^{-1}$ at 91.5 km, corresponding to a direction of propagation of either 6° or 186°.

Alternatively, we anticipate that the wave motion will have a maximum negative temperature gradient at the height at which the wave velocity is in the direction of propagation. This occurs at 85.4 and 115.4 km, where the inferred wave velocity is at 305°. Thus on the basis of the rocket data alone, there is considerable uncertainty in the direction of wave propagation because of the errors inherent in the wave velocity determinations and possible contamination by tidal modes. It is shown later, however, that a much more consistent picture of the wave motion emerges when the radar data are considered as well.

It was shown previously that the $\lambda_z \sim$ 30-km wave present in the rocket data corresponds to a low-frequency motion with a velocity field that rotates clockwise with height. This same character is observed in the radar velocity field shown in Figure 1. There is also evidence that these velocities rotate clockwise in time, providing an additional suggestion of a low-frequency wave motion. A least squares fit to the velocity field between 1200 and 2400 LT at each height was obtained for a wave period of 7 hours. The phases and amplitudes obtained for the "east" and "north" beams at each height are shown in Figure 7. These exhibit a clear phase progression with height, with an average phase difference of ~84° and an "east" velocity approximately 40% larger than the "north" velocity. There is also a tendency for each velocity component to increase in magnitude by ~30% over the ~6-km height interval, a factor much smaller than anticipated in the absence of dissipation for a scale height of ~4 km. Using these component velocities, we determine the velocity ellipse, and thus the wave amplitude and the apparent direction of propagation, at each height. Because the mean velocity has been removed at each level, this analysis yields a direction of propagation that is quite uniform with height and more reliable than that obtained using the rocket velocity and temperature data. The inferred direction of propagation is 222° ± 23°, approximately midway between those values determined using the rocket data.

The radar configuration also provides information on the vertical velocities due to gravity wave motions. For low-frequency motions, however, these velocities are of the order of the system resolution used during the STATE experiment. Because this results in significant errors in the estimates of amplitude and phase, these data are not used in this analysis.

We now proceed to calculate the ratio of observed wave amplitude relative to that required for monochromatic wave saturation [see *Fritts and Rastogi*, 1985]. From (6), this ratio may be expressed in terms of the wave velocity or temperature as

$$a \equiv \frac{u'}{(\bar{u} - c)} = \frac{T_z'}{(\bar{T}_z + g/c_p)} \tag{10}$$

Above the mesopause,

$$\bar{T}_z + g/c_p \approx 16°\text{C/km} \tag{11}$$

TABLE 1. Wave Parameters Inferred From Rocket and Radar Data for Large-Scale, Low-Frequency Wave Motion Present During Salvo 2 on June 15, 1983

| Parameter | Rocket | Radar |
|---|---|---|
| Data height interval, km | 85–130 | 83–89 |
| $\lambda_z$, km | 30 | ~70 |
| Period, hours | ... | ~17 |
| $T'$, A (°C)/height of max, km | 59.7/107.9 | ... |
| $u'$, A (m $s^{-1}$)/height of max, km | 42.2/98.1 | 40 ± 4/... (beam RX1) |
| $v'$, A (m $s^{-1}$)/height of max, km | 82.3/91.3 | 28 ± 3/... (beam RX2) |
| $\Delta\phi$, deg | 82 | 84 |
| $\lvert u' \rvert_{max}$, A (m $s^{-1}$)/height of max, km | 82.5/91.5 | 40 ± 4/... |
| Direction of $\lvert u \rvert_{max}$, deg | 6 or 186 | 222 ± 23 |
| Direction from $T'$ phase, deg | 305 | ... |
| Degree of saturation $u'/T_z'$ | 0.76/0.78 | 0.42 |
| Rotation with $z$ | clockwise | clockwise |
| Phase progression | downward | downward |

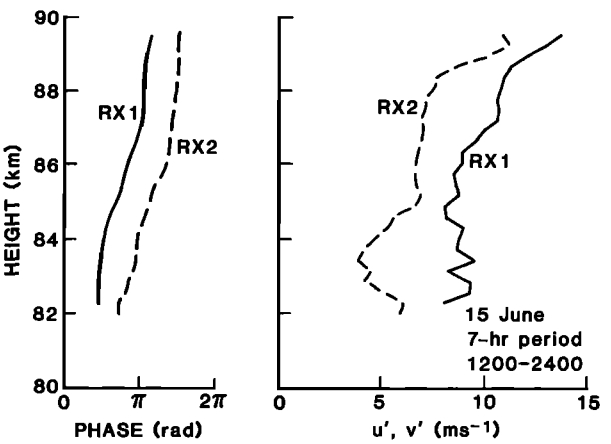


Fig. 7. Phases and amplitudes of the horizontal wind components for the 7-hour wave inferred from the radar data. Beams RX1 and RX2 are oriented 26° north of east and west of north, respectively. Phase increases with time.

and

$$|T_z'| = mT' = 12.5°\text{C/km} \tag{12}$$

yielding an estimate

$$a = 0.78 \tag{13}$$

Alternatively, with (11) and a mean temperature $\sim 300°$C, we obtain

$$N^2 = \frac{g}{\bar{T}}\left[\bar{T}_z + g/c_p\right] = 5.2 \times 10^{-4}\ \text{s}^{-2} \tag{14}$$

Together with

$$|u'|_{max} = 82.5\ \text{m s}^{-1} \tag{15}$$

and (4), this implies

$$|c - \bar{u}| = 109\ \text{m s}^{-1} \tag{16}$$

and

$$a = 0.76 \tag{17}$$

Thus despite the obvious uncertainties in our estimates of the wave parameters using the rocket temperature and velocity profiles, these independent estimates of wave amplitude are in remarkably good agreement.

A similar exercise using the radar data available at lower heights, with $\lambda_z \simeq 17$ km and $N^2 = 1.05 \times 10^{-3}\ \text{s}^{-2}$ (due to the much smaller mean temperature), yields

$$|c - \bar{u}| = 88\ \text{m s}^{-1} \tag{18}$$

and

$$a = 0.42 \tag{19}$$

The amplitude of the wave motion is smaller here, consistent with the observed growth with height in the radar data. Also, the vertical wavelength is compressed relative to that value inferred at upper levels because of the much larger stratification resulting from a small mean temperature and large mean temperature gradient immediately above the mesopause. It was this response to the thermal structure that led *Balsley et al.* [1983] to suggest that the summer mesopause should be a preferred site for gravity wave and tidal saturation and turbulence generation.

With the available radar data, we are also in a position to estimate the intrinsic period and the horizontal wavelength of the wave motion. Using (9) and the magnitudes of the perturbation velocities parallel and perpendicular to the direction of wave propagation, we find that

$$T_i = \frac{2\pi}{\omega} = \frac{2\pi|v'|}{f|u'|} \approx 8.8\ \text{hours} \tag{20}$$

The intrinsic period can also be estimated from the measured period, the intrinsic phase speed inferred from the vertical wave structure, and the magnitude and direction of the mean flow, 32 m s$^{-1}$ at 242°. This yields $\bar{u} \approx 30$ m s$^{-1}$ and

$$T_i = Tc/(c - \bar{u}) \approx 9.4\ \text{hours} \tag{21}$$

As in the case of wave amplitude, the consistency of these estimates suggests that the wave is described well by the radar data. With the intrinsic phase speed and frequency, the horizontal wavelength may be estimated, using (2) as

$$\lambda_x = \frac{2\pi}{k} = \frac{2\pi(c - \bar{u})}{\omega} \approx 3 \times 10^3\ \text{km} \tag{22}$$

As noted earlier, this low-frequency wave motion has several characteristics in common with anticipated tidal motions, including a near-tidal period, a fairly large vertical wavelength ($\lambda_z \gtrsim 17$ km), and a clockwise rotation of the velocity field with height and time. We believe, however, that the very sudden appearance of the wave motion, together with the consistency of the inferred wave structure, suggests that the wave is not a tidal motion. Our determination of the wave parameters may, nevertheless, have been affected to some degree by the presence of tidal components. We also note that the effects of this wave motion appear to be virtually identical to those attributed to tidal and low-frequency gravity wave motions near the summer mesopause by *Balsley et al.* [1983].

We now examine the consequences of a saturating wave field dominated by this 30-km wave motion. From the analysis presented by *Fritts and Rastogi* [1985], we see that a wave with $f/\omega = 0.72$ is dynamically unstable for

$$a \geqq 0.82 \tag{23}$$

Thus the 30-km wave at upper levels is nearly dynamically unstable, even in the absence of other wave motions. There is little doubt that the large-scale ($\lambda_z \gtrsim 5$ km) wave field is dynamically and/or convectively unstable at some locations when all components are considered.

At the level of radar observations, the 7-hour wave has an amplitude substantially less than that required for instability. This does not imply that the overall wave field is stable, however. Indeed, wave amplitudes smaller than monochromatic saturation values have been inferred in several observational studies of gravity wave saturation [*Smith and Fritts*, 1983; *Meek et al.*, 1985*a*; *Reid and Vincent*, 1987*a*], and the numerical study by *Fritts* [1985] indicates that saturation may occur at small wave amplitudes due to a superposition of waves.

Because the velocity field in the last $\sim 12$ hours of Figure 1 clearly is dominated by the 7-hour wave, it seems appropriate to ask whether this motion is related to the occurrence of strong radar echoes and to the turbulence enhancements thought to be responsible for these echoes. To answer this question, we have shown contours of S/N above 0 dB for this period in Figure 8. As suggested by the velocity field in Figure 1, regions of maximum S/N appear as descending layers about 7 hours apart, indicating a strong correlation with the 7-hour wave motion. This correlation is further enhanced if we plot the phase of the wave motion corresponding to the most unstable portion of the wave field anticipated from the discussion in section 2. These are shown by the solid lines in Figure 8 and indicate the locations in the wave field where the temperature gradient is most negative and where the perturbation velocity is in the direction of wave propagation (222°), as seen in Figure 1. Thus the radar data provide strong evidence of a significant enhancement in turbulence activity at precisely that phase of the wave motion where instability and dissipation are expected to occur on theoretical grounds. Further evidence of this correlation is provided by the findings of *Watkins et al.* [1987], in which the height of the maximum inferred energy dissipation rate was observed to descend with time and to coincide with the maximum in S/N in Figure 8.

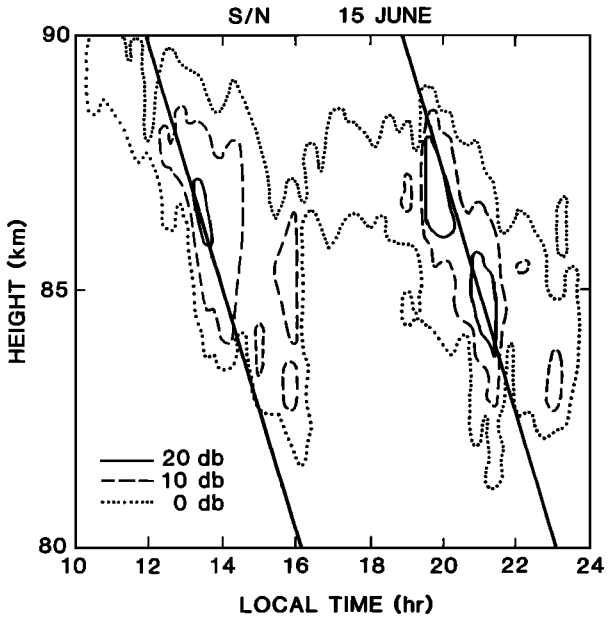


Fig. 8. Time-height cross section of radar S/N for June 15, from 1000 to 2400 LT. The slanted lines denote the most unstable phase of the 7-hour wave inferred from the temperature and velocity data and correlate well with regions of maximum S/N.

This observation has significant implications for the diffusion of heat and constituents and suggests a large effective Prandtl number at these heights [*Chao and Schoeberl*, 1984; *Fritts and Dunkerton*, 1985; *Strobel et al.*, 1985]. It should again be stressed that this phase of the wave motion corresponds to a minimum of the perturbation velocity shear.

Returning to the differenced rocket temperature and velocity data (Figures 5 and 6), we see that there is a tendency for enhanced small-scale wave structure ($\lambda_z \sim 2$–3 km) to occur near those heights where the temperature gradient associated with the 7-hour wave is most negative (~85 and 115 km). This suggests that large-scale wave motions act as a source of both turbulence and small-scale wave activity preferentially in regions where the wave field is most unstable. In the present case, it appears that this is a result of a dynamical instability of the flow, as described earlier in this section. This conclusion is supported by the lack of large-scale superadiabatic lapse rates in the rocket temperature data (see Figure 6). In other cases of gravity wave saturation involving wave motions with high intrinsic frequencies, it appears that turbulence and wave excitation occur primarily as the result of a convective instability [*Fritts*, 1984*a*; *Fritts and Rastogi*, 1985]. These observations are in qualitative agreement with numerical studies suggesting that both dynamical and convective instabilities may lead to the excitation of other internal gravity wave motions [*Fritts*, 1984*b*, 1985; *Chimonas and Grant*, 1984]. Finally, another process that may be important in the evolution of a saturating gravity wave spectrum [*Weinstock*, 1982], but which appears not to prevent the occurrence of wave field instability [*Fritts*, 1985; *Smith et al.*, 1987], is the nonlinear interaction of waves that have attained large amplitudes.

### 4.2. *The $\lambda_z \sim$ 2- and 12-km Waves*

As is apparent from the discussion in section 2 and Figures 1–4, the rocket and radar data collected during salvo 2 contain evidence of a wide range of wave motions occurring at various temporal and spatial scales. The focus earlier in this section was on the 30-km wave present at upper levels because of the dominant role it obviously played in the dynamics. However, other motions are likely to be equally important at lower levels where the 30-km wave has not approached a saturated amplitude.

One such motion, occurring at the height of the radar echo and appearing in both zonal and meridional rocket velocity profiles (see Figure 3), is found to have a least squares vertical wavelength of $\lambda_z = 12$ km in the interval from 75 to 95 km. As in the case of the 30-km wave, this motion is assumed to be saturated and thus to have a constant amplitude with height. The parameters estimated for this 12-km wave are listed in Table 2.

The zonal and meridional velocity components are seen to be nearly in phase, suggesting a high-frequency motion of horizontal magnitude 19.9 m $s^{-1}$ propagating toward 41°. A similar fit to the temperature data yielded an amplitude of 7.6°C and a phase which, together with the velocity data, suggested a propagation toward 358°. It must be noted, however, that the estimate of temperature amplitude is subject to considerable error because of the mean thermal structure near the mesopause. Nevertheless, we estimate the wave amplitude relative to the saturated value as before, assuming $N^2 = 6.4 \times 10^{-4}$ $s^{-2}$, and obtain ratios of 0.41 and 0.77 from the velocity and temperature data, respectively. In this case, the stratification experienced by the high-frequency motion is assumed to be that due to the mean state and the 7-hour wave motion. These results suggest that this motion may contribute significantly to the attainment of a saturated wave field at the heights of the radar echoes. In particular, this high-frequency motion may be the cause of some of the rapidly descending S/N maxima embedded within the dominant 7-hour periodicity seen in Figure 8. These maxima suggest a wave period of ~1 hour, but because of the large-amplitude 7-hour motion, no such period was conspicuous in the radar data.

One final wave motion in the salvo 2 data that warrants some discussion is the very conspicuous $\lambda_z \sim$ 2-km structure seen in the temperature gradient data in Figure 6. The small vertical wavelengths (and small intrinsic phase speeds) of these motions suggest that they must have been generated locally. Additionally, the very large (convectively unstable) amplitudes occurring near the minima of the large-scale $dT/dz$ profile imply that such motions are generated preferentially where the

TABLE 2. Wave Parameters Inferred From Rocket Data for the $\lambda_z$ ~12 km Wave Motion Observed at Intermediate Heights During Salvo 2 on June 15, 1983

| Parameter | Rocket |
|---|---|
| Data height interval, km | 75–95 |
| $\lambda_z$, km | 12 |
| Period (intrinsic) | short |
| $T'$, A (°C)/height of max, km | 7.6/96.6 |
| $u'$, A (m $s^{-1}$)/height of max, km | 13.4/89.4 |
| $v'$, A (m $s^{-1}$)/height of max, km | 15.2/88.7 |
| $\Delta\phi$, deg | 22 |
| $\lvert u'\rvert$, A (m $s^{-1}$)/height of max, km | 19.9/89.0 |
| Direction of $\lvert u'\rvert_{max}$, deg | 41 |
| Direction from $T'$ phase, deg | 358 |
| Degree of saturation $u'/T_z'$ | 0.41/0.77 |

Wave motion was not distinguishable from the low-frequency motion in the radar data.

large-scale wave field is unstable. Because the small-scale motions are themselves forced to unstable amplitudes, they contribute to the generation of turbulence and the cascade of wave energy to smaller scales.

## 5. Analysis of June 17 Radar Data

As described in section 2, the radar velocity field obtained on June 17 exhibits a pronounced wave motion and a corresponding modulation of the echo occurrence (and intensity) at lower levels with a period of ~3 hours (see Figure 2). This is very similar to the correlation between the velocity field and echo occurrence observed for the 7-hour wave during salvo 2 and analyzed in section 4. The purpose of this section is to determine whether the enhanced echoes can again be related to the most unstable portion of the wave field.

A least squares fit to the velocity data between ~83 and 88 km from 0400 to 1000 LT was obtained for a wave period $T = 190$ min. This wave motion is also observed above and below this height interval, but a lack of sufficient echo leads to a reduction in the number of accepted data points and a degradation of the fit at these heights. The phase of the motion in the two radar beams is shown as a function of height in Figure 9. From these data we infer a vertical wavelength of ~38 km and a corresponding intrinsic phase speed of ~150 m s$^{-1}$, though there is some uncertainty in these estimates due to the different phase slopes in the two beams. The magnitude of the velocity fluctuation and the inferred direction of propagation are shown as functions of height in Figure 10. These data suggest an increase of wave amplitude with height from ~20 m s$^{-1}$ at 83 km to ~26 m s$^{-1}$ at 86 km and a direction of propagation of ~205°. The increase in wave amplitude with height is less than that required for conservative wave motion, suggesting that the wave is likely to be dissipating and contributing to the occurrence of the radar echoes at these heights.

The mean flow inferred between 84 and 86 km is ~60 m s$^{-1}$ at 246°. The component of this flow in the direction of wave propagation is $\bar{u} \sim 45$ m s$^{-1}$, which, with the estimated intrinsic phase speed, implies a phase speed $c \sim 195$ m s$^{-1}$ and a horizontal wavelength

$$\lambda_x = cT \sim 2230 \text{ km} \tag{24}$$

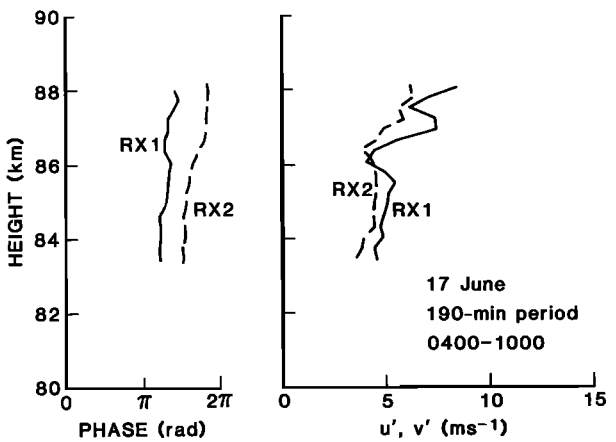


Fig. 9. Phases and amplitudes of the horizontal wind components for the 190-min wave seen in the radar data on June 17. Phase increases with time.

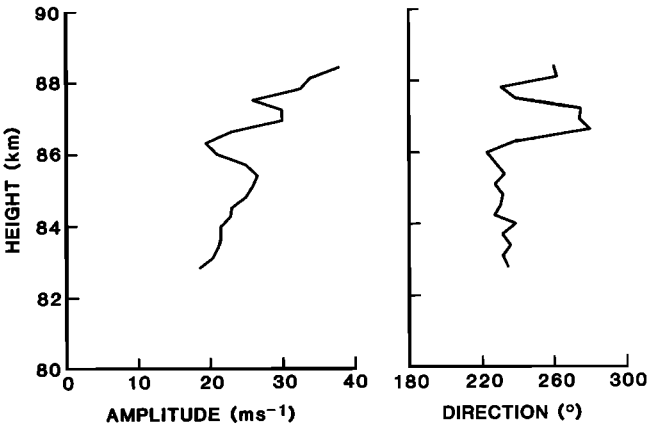


Fig. 10. Magnitude and direction of the horizontal motion for the 190-min wave. Note that the direction of propagation corresponds to the perturbation velocity at levels where the S/N is enhanced.

This suggests an intrinsic period

$$T_i = \frac{2\pi}{k(c - \bar{u})} \sim 247 \text{ min} \tag{25}$$

It must be recognized, however, that these values reflect the uncertainty in our estimate of the vertical wavelength of the wave motion and are likely to be less accurate than those values estimated using rocket and radar data in section 4.

Thus we have again obtained a reasonably consistent description of the wave field on the basis of the available radar velocity data. This view is reinforced by noting that the phase of the wave motion in which the S/N (and presumably instability and turbulence) is enhanced corresponds, as in the case of the 7-hour wave, to that which is expected to be most unstable on the basis of the discussion in section 3. This results in perturbation velocities at the lowest echoing levels that are in the direction of wave propagation, suggesting an easy way to infer this quantity in other data.

## 6. Summary and Conclusions

We have presented analyses of several gravity wave motions observed in the mesosphere and lower thermosphere using data collected during the STATE experiment. This experiment was designed to examine the conditions responsible for the strong Poker Flat MST radar echoes occurring near the summer mesopause. The rocket and radar data obtained have provided a unique picture of both the spatial and temporal structure of the gravity wave field present at the time of the experiment.

The combined rocket and radar temperature and velocity data collected during salvo 2 on June 15 were found to permit a more complete specification of the wave field than could have been accomplished using either system alone. Clearly the dominant motion was the large-scale, low-frequency wave observed by both systems. Using the rocket data at upper levels and the radar data near the mesopause and assuming a gravity wave rather than a tidal structure, it was possible to infer all of the principal wave parameters including amplitude, horizontal and vertical wavelength, phase speed, intrinsic period, and direction of propagation. Specifically, this wave motion was found to have an amplitude comparable to that required for dynamical instability at upper levels. Near the mesopause

that phase of the wave that was expected to be most unstable, based on the inferred wave structure, was found to correlate very well with enhanced S/N in the radar data (and presumably with increased instability and turbulence), suggesting that the generation of intense turbulence is highly localized within the wave field and thus that the Prandtl number due to wave-generated turbulence is large [*Fritts and Dunkerton*, 1985]. This wave was estimated to propagate toward the southwest.

A second wave motion with a vertical wavelength $\lambda_z \sim 12$ km was also deduced using the rocket data near the mesopause. The amplitude of this motion was estimated to be sufficient to contribute appreciably to the saturation of the low-frequency wave motion in this region. A high intrinsic frequency was inferred both from the phase consistency between the zonal and meridional velocities and from the high-frequency ($T \sim 1$ hour) modulation of the radar S/N data. Finally, this wave motion was found to propagate toward the north.

Also conspicuous in the rocket temperature gradient data, in particular, were wave motions with $\lambda_z \sim 2$ km. These were observed with extremely large (unstable) amplitudes near regions in which the large-scale wave field was itself most unstable. The very slow vertical propagation and large rate of dissipation anticipated for such motions further suggest that they may result from the instability of the large-scale wave field.

Another low-frequency event observed in the radar data on June 17 was analyzed because it appeared to be related to a modulation of the lowest heights from which useful radar echoes were obtained. This wave had a period $T \sim 190$ min, with clearly defined amplitude and phase near the mesopause, permitting a fairly unambiguous specification of the wave structure. As in the case of the 7-hour wave, a strong correlation between the most unstable phase of the wave motion and the occurrence of large S/N was observed, providing further evidence that turbulence generation is localized within the wave field. This wave motion was found to propagate toward the south-southwest.

The data analyses presented here suggest that occurrences of gravity wave saturation in the mesosphere and lower thermosphere are largely consistent with theoretical expectations of saturation via a dynamical or convective instability of the wave field [*Hodges*, 1967; *Lindzen*, 1981; *Fritts and Rastogi*, 1985]. For large-scale motions there was found to be a strong correlation between large radar S/N (and large inferred turbulence intensities) and the most unstable phase of the wave motion. This suggests that turbulence generation and effects may be strongly localized within the wave field, perhaps resulting in a large effective Prandtl number, as anticipated by *Chao and Schoeberl* [1984] and *Fritts and Dunkerton* [1985]. Evidence was also found of the excitation of other gravity wave motions at small scales preferentially near regions of maximum instability of the large-scale wave field. Whether these motions were the results of wave-wave interactions of the sort considered by *Weinstock* [1982] and *Fritts* [1985] or a consequence of dynamical or convective instabilities [*Fritts*, 1984*b*, 1985] could not be determined.

It should also be noted that there is a tendency to select for analysis those wave motions with the largest amplitudes and hence the largest vertical wavelengths and intrinsic phase speeds. These motions are expected, because of their large energies and large vertical group velocities, to be the most significant in terms of turbulence production. However, motions with small intrinsic frequencies are not expected to contribute appreciably to the transport of momentum because of their relatively small vertical perturbation velocities [*Vincent and Reid*, 1983; *Fritts*, 1984*a*]. Indeed, those motions analyzed in this paper were propagating toward the north or the southwest and thus could not have contributed appreciably to the deceleration of the mean easterly flow in the mesosphere. Because of this and other related data [*Smith and Fritts*, 1983; *Meek et al.*, 1985*b*; *Vincent and Fritts*, 1987], it would appear essential to consider those factors affecting the meridional as well as the zonal propagation of gravity waves in any comprehensive treatment of gravity wave effects in the middle atmosphere. This element of the problem has been largely neglected in most studies to date.

*Acknowledgments.* This work was supported by the Air Force Office of Scientific Research (AFSC) under grant AFOSR-82-0125 and contract F49620-87-C-0024. The authors are grateful to Mark Schoeberl and one anonymous reviewer for helpful comments on the manuscript.

## REFERENCES

Balsley, B. B., W. L. Ecklund, and D. C. Fritts, VHF echoes from the high-latitude mesosphere and lower thermosphere: Observations and interpretations, *J. Atmos. Sci.*, *40*, 2451–2466, 1983.

Chao, W. C., and M. R. Schoeberl, A note on the linear approximation of gravity wave saturation in the mesosphere, *J. Atmos. Sci.*, *41*, 1893–1898, 1984.

Chimonas, G., and J. R. Grant, Shear excitation of gravity waves, II, Upscale scattering from Kelvin-Helmholtz waves, *J. Atmos. Sci.*, *41*, 2278–2288, 1984.

Dunkerton, T. J., Stochastic parameterization of gravity wave stresses, *J. Atmos. Sci.*, *39*, 1711–1725, 1982*a*.

Dunkerton, T. J., Wave transience in a compressible atmosphere, III, The saturation of internal gravity waves in the mesosphere, *J. Atmos. Sci.*, *39*, 1042–1051, 1982*b*.

Dunkerton, T. J., and D. C. Fritts, Transient gravity wave critical layer interaction, I, Convective adjustment and the mean zonal acceleration, *J. Atmos. Sci.*, *41*, 992–1007, 1984.

Fritts, D. C., Gravity wave saturation in the middle atmosphere: A review of theory and observations, *Rev. Geophys.*, *22*, 275–308, 1984*a*.

Fritts, D. C., Shear excitation of atmospheric gravity waves, II, Nonlinear radiation from a free shear layer, *J. Atmos. Sci.*, *41*, 524–537, 1984*b*.

Fritts, D. C., A numerical study of gravity wave saturation: Nonlinear and multiple-wave effects, *J. Atmos. Sci.*, *42*, 2043–2058, 1985.

Fritts, D. C., and T. J. Dunkerton, Fluxes of heat and constituents due to convectively unstable gravity waves, *J. Atmos. Sci.*, *42*, 549–556, 1985.

Fritts, D. C., and P. K. Rastogi, Convective and dynamical instabilities due to gravity wave motions in the lower and middle atmosphere: Theory and observations, *Radio Sci.*, *20*, 1247–1277, 1985.

Fritts, D. C., and R. A. Vincent, Mesospheric momentum flux studies at Adelaide, Australia: Observations and a gravity wave/tidal interaction model, *J. Atmos. Sci.*, *44*, 605–619, 1987.

Hodges, R. R., Jr., Generation of turbulence in the upper atmosphere by internal gravity waves, *J. Geophys. Res.*, *72*, 3455–3458, 1967.

Holton, J. R., The role of gravity wave induced drag and diffusion in the momentum budget of the mesosphere, *J. Atmos. Sci.*, *39*, 791–799, 1982.

Holton, J. R., The influence of gravity wave breaking on the general circulation of the middle atmosphere, *J. Atmos. Sci.*, *40*, 2497–2507, 1983.

Houghton, J. T., The stratosphere and mesosphere, *Q. J. R. Meteorol. Soc.*, *104*, 1–29, 1978.

Kelley, M. C., J. C. Ulwick, and K. D. Baker, Large- and small-scale organization of electrons in the high-latitude mesosphere: Implications of the STATE data, *J. Geophys. Res.*, this issue.

Lindzen, R. S., Turbulence and stress owing to gravity wave and tidal breakdown, *J. Geophys. Res.*, *86*, 9707–9714, 1981.

Matsuno, T., A quasi-one-dimensional model of the middle atmosphere circulation interacting with internal gravity waves, *J. Meteorol. Soc. Jpn.*, *60*, 215–226, 1982.

Meek, C. E., I. M. Reid, and A. H. Manson, Observations of mesospheric wind velocities, 1, Gravity wave horizontal scales and phase velocities determined from spaced wind observations, *Radio Sci.*, *20*, 1363–1382, 1985*a*.

Meek, C. E., I. M. Reid, and A. H. Manson, Observations of mesospheric wind velocities, 2, Cross sections of power spectral density for 48-8 hours, 8-1 hours, 1 hour to 10 min over 60-110 km for 1981, *Radio Sci.*, *20*, 1383–1402, 1985*b*.

Miyahara, S., Y. Hayashi, and J. D. Mahlman, Interactions between gravity waves and planetary scale flow simulated by the GFDL "SKYHI" general circulation model, *J. Atmos. Sci.*, *43*, 1844–1861, 1986.

Reid, I. M., and R. A. Vincent, Measurements of the horizontal scales and phase velocities of short-period mesospheric gravity waves at Adelaide, Australia, *J. Atmos. Terr. Phys.*, *49*, 1033–1048, 1987*a*.

Reid, I. M., and R. A. Vincent, Measurements of mesospheric gravity wave momentum fluxes and mean flow accelerations at Adelaide, Australia, *J. Atmos. Terr. Phys.*, *49*, 443–460, 1987*b*.

Schoeberl, M. R., D. F. Strobel, and J. P. Apruzese, A numerical model of gravity wave breaking and stress in the mesosphere, *J. Geophys. Res.*, *88*, 5249–5259, 1983.

Smith, S. A., and D. C. Fritts, Estimation of gravity wave motions, momentum fluxes and induced mean flow accelerations in the winter mesosphere over Poker Flat, Alaska, in *Proceedings of the 21st Conference on Radar Meteorology*, pp. 104–110, American Meteorological Society, Boston, Mass., 1983.

Smith, S. A., D. C. Fritts, and T. E. VanZandt, Evidence of a saturated spectrum of atmospheric gravity waves, *J. Atmos. Sci.*, *44*, 1404–1410, 1987.

Strobel, D. F., J. P. Apruzese, and M. R. Schoeberl, Energy balance constraints on gravity wave induced eddy diffusion in the mesosphere and lower thermosphere, *J. Geophys. Res.*, *90*, 13,067–13,072, 1985.

Ulwick, J. C., M. C. Kelley, K. D. Baker, B. B. Balsley, and W. C. Ecklund, Comparison of simultaneous MST radar and electron density probe measurements during STATE, *J. Geophys. Res.*, this issue.

Vincent, R. A., Gravity wave motions in the mesosphere, *J. Atmos. Terr. Phys.*, *46*, 119–128, 1984.

Vincent, R. A., and D. C. Fritts, A climatology of gravity wave motions in the mesosphere at Adelaide, Australia, *J. Atmos. Sci.*, *44*, 748–760, 1987.

Vincent, R. A., and I. M. Reid, HF Doppler measurements of mesospheric gravity wave momentum fluxes, *J. Atmos. Sci.*, *40*, 1321–1333, 1983.

Walterscheid, R. L., Gravity wave attenuation and the evolution of the mean state following breakdown, in *Dynamics of the Middle Atmosphere*, edited by J. R. Holton and T. Matsuno, pp. 19–44, Terra Scientific, 1984.

Watkins, B. J., C. R. Philbrick, and B. B. Balsley, Turbulence energy dissipation rates and inner scale sizes from rocket and radar data, *J. Geophys. Res.*, this issue.

Weinstock, J., Nonlinear theory of gravity waves: Momentum deposition, generalized Rayleigh friction and diffusion, *J. Atmos. Sci.*, *39*, 1698–1710, 1982.

B. B. Balsley, Aeronomy Laboratory, National Oceanic and Atmospheric Administration, 325 Broadway, Boulder, CO 80303.

D. C. Fritts, Geophysical Institute, University of Alaska, Fairbanks, AL 99775.

C. R. Philbrick, Air Force Geophysics Laboratory, Hanscom Air Force Base, Bedford, MA 01731.

S. A. Smith, NASA Marshall Space Flight Center, Huntsville, AL 35812.

(Received October 27, 1986;
revised June 7, 1987;
accepted June 9, 1987.)